Goulet, J., Michel, C., and Smith, I. (2013). Hybrid probabilities and error-domain structural identification using ambient vibration monitoring. Mechanical Systems and Signal Processing, 37(1–2):199–212.
http://dx.doi.org/10.1016/j.ymssp.2012.05.017

Hybrid probabilities and error-domain structural identification using ambient vibration monitoring

James-A. Goulet[a,*], Clotaire Michel[b], Ian F. C. Smith[a]

[a]*Applied Computing and Mechanics Laboratory (IMAC)*
School of Architecture, Civil and Environmental Engineering (ENAC)
ÉCOLE POLYTECHNIQUE FÉDÉRALE DE LAUSANNE (EPFL)
Lausanne, Switzerland
[b]*Swiss Seismological Service (SED)*
SWISS FEDERAL INSTITUTE OF TECHNOLOGY ZURICH *(ETHZ)*
Zurich, Switzerland

Abstract

For the assessment of structural behavior, many approaches are available to compare model predictions with measurements. However, few approaches include uncertainties along with dependencies associated with models and observations. In this paper, an error-domain structural identification approach is proposed using ambient vibration monitoring (AVM) as the input. This approach is based on the principle that in science, data cannot truly validate an hypothesis, it can only be used to falsity it. Error-domain model falsification generates a space of possible model instances (combination of parameters), obtains predictions for each of them and then, rejects instances that have unlikely differences (residuals) between predictions and measurements. Models are filtered in a two step process. Firstly a comparison of mode shapes based on MAC criterion ensures that the same modes are compared. Secondly, the frequencies from each model instance are compared with the measurements. The instances for which the difference between the predicted and measured value lie outside threshold bounds are discarded. In order to include "uncertainty of uncertainty" in the identification process, a hybrid probability scheme is also presented. The approach is used for the identification of the Langensand Bridge in Switzerland. It is used to falsify the hypothesis that the bridge was behaving as designed when subjected to ambient vibration inputs, before opening to the traffic. Such small amplitudes may be affected by low-level bearing-device friction. This inadvertently increased the apparent stiffness of the structure by 17%. This observation supports the premiss that ambient vibration surveys

*Corresponding author: james.a.goulet@gmail.com

should be cross-checked with other information sources, such as numerical models, in order to avoid misinterpreting the data.

Keywords: Structural identification, Ambient vibration monitoring, Uncertainty, error-domain identification, Extended uniform distribution, Correlation, Error

1. Introduction

In the early history of dynamic monitoring of bridges, researchers were interested in the modal properties of these structures. For instance Carder [11], used monitoring to predict resonance during an earthquake. From the 70s, the development of recording capabilities (e.g. [27]) and of numerical modelling lead researchers to validate bridge models using experimental ambient vibration data [1]. Later, researchers began optimizing model parameters to improve the fit between predicted and observed data. Mottershead and Friswell [32] reviewed some of these applications. Since then, there has been an increasing popularity for Bayesian-updating methodologies [3, 4]. Many applications of dynamic monitoring of bridges can be found in the literature, for example [3, 9, 13, 14, 23, 26, 31, 33, 38, 40, 41, 46, 49]. Some of these studies, such as [3] and [14], explicitly included uncertainties in the identification process. These studies however did not include modelling uncertainties due to aspects such as model simplification, omissions and mesh refinement.

Error-domain model falsification was proposed by Goulet and Smith [19] for situations where bias in models introduce dependencies between predictions. This approach is based on the principle that in science, data cannot convincingly validate an hypothesis, it can only be used to falsity it [36, 45]. Error-domain model falsification is built upon more than a decade of research [37, 39, 43]. In a previous study [17], a similar identification approach was used to perform structural identification on bridges based on static measurements. Error-domain identification was proposed to overcome the limitations of other approaches based on statistical inference that relies on the correct evaluation of uncertainties and of their dependencies [5, 44]. Error-domain model falsification generates a space of possible model instances (combination of parameters), obtains predictions and then falsifies wrong instances based on the difference between predictions and measurements (*observed residual*). A model instance is falsified, if the observed residuals lies outside threshold bounds computed from the combination of modelling and measurement uncertainties.

Elements of error-domain model falsification is presented in Equations 1 to 3. A model class $\mathbf{g}(\vec{\theta})$ is used to perform predictions based on vector containing n_p input parameters $\vec{\theta} = [\theta_1, \theta_2, \theta_3, \ldots, \theta_{n_p}]$. If real quantities for these parameter are known $\vec{\theta}^*$, the difference between the value predicted by the model and the modelling error ϵ_{model} is equal to the physical quantity $\mathcal{R}$ for the system (see Equation 1). The difference between the measured value y and the measurement error $\epsilon_{measure}$ is also equal to this physical quantity. In practical situations, neither errors nor the real physical quantity is available.

$$\mathbf{g}(\vec{\theta}^*) - \epsilon_{model} = \mathcal{R} = y - \epsilon_{measure} \tag{1}$$

In Equation 2, exact values of errors are replaced by a random variables U_{model} and $U_{measure}$ each described by a probability density function (PDF) $f_U(\epsilon) : \mathbb{R} \to \mathbb{R}_+$. The relation used to falsify models can be obtained by reordering the terms in Equation 3. In this Equation, the left-hand term is the *observed residual* of the difference between predicted and measured value and the right-hand term is a combined probability density function f_{U_c} representing modelling and measurement uncertainties. Uncertainty sources are combined using Monte-Carlo methods [15].

$$\mathbf{g}(\vec{\theta}) - U_{model} = y - U_{measure} \tag{2}$$

$$\mathbf{g}(\vec{\theta}) - y = U_{model} - U_{measure} \tag{3}$$

A model instance (i.e. a set of parameter values) $\vec{\theta}$ is falsified if the observed residual $\mathbf{g}(\vec{\theta}) - y$ lies outside the interval defined by threshold bounds $[T_{low}, T_{high}]$ as presented in Figure 1.

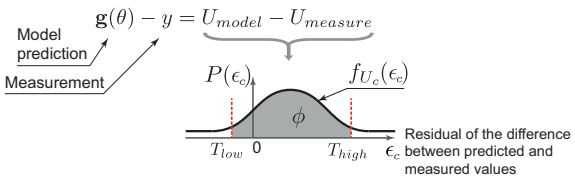

Figure 1: The combined probability density function describes the outcome of the random variable U_c. Threshold bounds $[T_{low}, T_{high}]$ represent the narrowest intervals that contains a target identification probability ϕ.

When using several measurement locations (comparison point) $i \in [1, \ldots, n_m]$, a model instance is falsified if the observed residual lies outside threshold bounds at *any* location. This condition is presented in Equation 4.

$$\forall i \in [1, \ldots, n_m] : \; T_{low,i} \leq \mathbf{g}(\vec{\theta}, i) - y_i \leq T_{high,i} \tag{4}$$

Threshold bounds are computed as the shortest intervals that contain a probability content $\phi \in]0 \ldots 1]$. This can be solved by satisfying the relation presented in Equation 5 for the domain $\mathcal{T} = [T_{low,1}, T_{high,1}] \times [T_{low,2}, T_{high,2}] \times \ldots \times [T_{low,n_m}, T_{high,n_m}] \subseteq \mathbb{R}^{n_m}$.

$$\forall i \in [1, \ldots, n_m] : \; \phi = \int \ldots \int_{\mathcal{T}} f_{U_{c,i}}(\epsilon_{c,1}, \ldots, \epsilon_{c,n_m}) d\epsilon_{c,1} \ldots d\epsilon_{c,n_m} \tag{5}$$

Here, combining modeling and measurement uncertainties allows determination of the maximal plausible errors (Threshold bounds) for a target reliability ϕ. Thus, there is a probability $< 1 - \phi$ of wrongly rejecting correct models. Some wrong models are likely to be kept in the candidate model set if they are close enough to measured data. This procedure is intended to be conservative because all candidate models are considered as possible explanations of the behavior. Accepting false models is in most cases inevitable in order to ensure that the right model will not be wrongly discarded.

As suggested by Beven [6], a model class $\mathbf{g}(\ldots)$ is falsified when all its model instances $\vec{\theta}$ are falsified by threshold bounds. Falsifying an entire model class is an indication that there are flaws in the way the system is modeled. No other methodology in use for structural identification is capable of detecting wrong model classes.

Uncertainty quantification is a task intrinsic to system identification. In addition to the traditional probabilistic description of uncertainties, other approaches, such as interval analysis [30] and probability bounds analysis [16, 42], have also been used to describe imprecise knowledge associated with uncertainties. These alternative approaches for defining and combining uncertainties are conservative [20]. In the case of system identification, these approaches can be too conservative, hindering the process of making sense out of data. When using probability density functions for describing uncertainties, in many cases, little information is available to accurately quantify them. The Uniform distribution may not reflect the subjective process of defining uncertainty bounds. For these situations, the curvilinear and iso-curvilinear distribution [22, 25]

have been proposed. When Uniform distributions are used to describe uncertainties, an uncertainty can also be associated with bound positions. When combined together, these distributions form the curvilinear distributions as presented in Figure 2. The uncertainty associated with bound positions is, however, also incomplete.

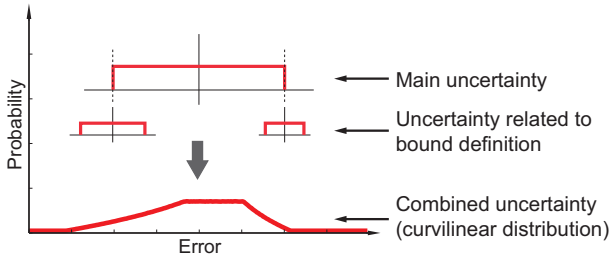

Figure 2: Curvilinear distribution that included uncertainty in bound position

In this paper, error-domain model falsification is further developed to allow the use of ambient vibration monitoring as the input during structural identification. Also, a new probability distribution is proposed to include the uncertainty involved with the inexact knowledge of the bounds of uniform distributions. Section 2 describes the fundamentals behind the use of dynamic input for system identification. This methodology is applied to a case study to confirm its applicability for identifying the behavior of full-scale structures.

2. Error-domain model falsification using ambient vibration monitoring

Experimental modal analysis is not a direct measurement of a physical parameter (displacement, rotation) but a relatively complex signal processing method allowing the modal parameters of a structure to be derived, including resonance frequencies, modal shapes and damping ratios. This analysis is based on the assumption of linear behaviour. Moreover, Operational Modal Analysis, i.e. under ambient vibrations, assumes that the input motion is of equal amplitude for every frequency (white noise) and that the recorded data averaged over a sufficient length of time is a direct representation of structural behaviour (stationary signal).

In this paper, the structural identification process is performed on the resonance frequencies only. However, in order to compare the predicted and measured frequencies, a correspondence check must be performed between the measured ($\Phi_{y,j}, j \in [1, \ldots, n_j]$) and predicted ($\Phi_{\mathbf{g}(\vec{\theta},k)}, k \in [1, \ldots, n_k]$) mode shapes in order to ensure that only the

corresponding modes are compared together. When dealing with large finite-element models, the number of predicted modes n_k is, in most situations, much larger than what is measured n_j. Moreover, the order of these modes may be different from one model instance ($\vec{\theta}_l$) to another. The Modal Assurance Criterion (MAC) [2] (Equation 6, where ^{H} denotes complex conjugate and transpose), is used to perform mode shapes correspondence checks in a first step. When the frequencies corresponding to each mode shape are found, model falsification is performed based on the observed and predicted frequencies.

$$\mathrm{MAC}(\Phi_{y,j}, \Phi_{\mathbf{g}(\vec{\theta}_l,k)}) = \frac{|\Phi_{y,j}^H \Phi_{\mathbf{g}(\vec{\theta}_l,k)}|^2}{|\Phi_{y,j}^H \Phi_{y,j}||\Phi_{\mathbf{g}(\vec{\theta}_l,k)}^H \Phi_{\mathbf{g}(\vec{\theta}_l,k)}|} \tag{6}$$

In order to identify the behavior of a structure, a set containing n_l model instances $\vec{\theta}_l, l \in [1,\ldots,n_l]$ is generated to explore the domain of possible solutions. Only sets $\{j,k,l\}$ satisfying Equation 7 $\forall j \in [1,\ldots,n_j], k \in [1,\ldots,n_k], l \in [1,\ldots,n_l]$ are used to falsify model instances. $\phi_{\mathrm{MAC}} \in [0,1]$ is the modal assurance criterion target defined by users.

$$\{(j,k,l) \in \mathbb{N}^3 : \ \mathrm{MAC}(\Phi_{y,j}, \Phi_{\mathbf{g}(\vec{\theta}_l,k)}) \geq \phi_{\mathrm{MAC}}\} \tag{7}$$

For some model instances $\vec{\theta}$, not all measured ($\Phi_{y,j}$) and predicted ($\Phi_{\mathbf{g}(\vec{\theta},k)}$) modes may pass the MAC correspondence test. Therefore, model falsification may not employ the same number of modes for all model instances. This approach is conservative because the confidence interval $T_{i,Low}$ and $T_{i,High}$ expressed in Equation 5 are determined using the full set containing $n_m = n_j$ measured modes. This strategy thereby extends the applicability of error domain model falsification to dynamic monitoring. A case-study is presented in Section 4. The goal of the identification is to falsify inappropriate hypotheses regarding the boundary conditions and material properties of the structure, for refining the set of models that may explain its behaviour.

3. Extended uniform distribution

Quantifying uncertainties is a task intrinsic to structural identification. Uniform distributions are often used to describe uncertainties related to model predictions. In these cases, lower and upper bounds $[A,B]$ are provided according to the subjective knowledge of experts. This is called the zero-order uncertainty ($n = 0$). An additional

order of uncertainty ($n = 1$) can be provided to include the uncertainty in the position of the zero-order uncertainty bounds. This process can go on for several orders of uncertainty, see Figure 3.

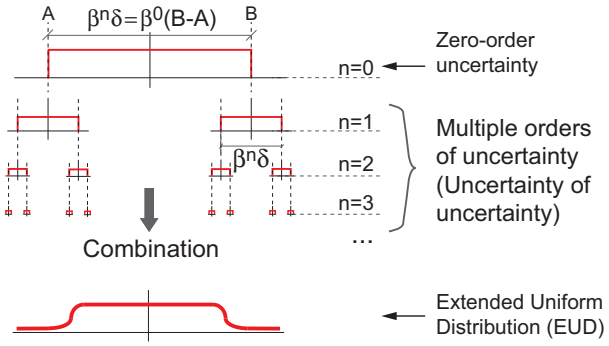

Figure 3: Extended uniform distribution that included several orders of uncertainty

Each distribution associated with multiple orders of uncertainty can be defined independently. However, for practical applications, defining a upper and lower bounds for each order of uncertainty is not feasible. A simplified method for defining the multiple orders of uncertainty is to define each n^{th} order of uncertainty as a fraction $\beta \in [0, 1]$ of the $n-1$ order of uncertainty. This fraction β defines the width of the n^{th} order of uncertainty using the relation $\beta^n \delta$, where $\delta = B - A$, is the interval width of the zero-order uncertainty. Thus the extended uniform distribution (EUD) can be generated by combining the zero-order uncertainty distributions with all higher-order distribution defined. Details regarding numerical methods available to combine these uncertainty distributions are presented by ISO guidelines [21]. Such combination transforms the initial zero-order uncertainty, having sharply defined bound, into a distribution representing the incomplete information of bound positions. The extended uniform distribution is presented in Figure 3.

For any value of β smaller than one, the distribution converges to a finite limit L expressed in Equation 8. This equation is the sum of the highest outcome of an infinite number of orders of uncertainty. As n becomes large, the contribution of orders tends to zero.

$$L = \frac{\beta^0(B-A)}{2} + \frac{\beta^1(B-A)}{2} + \ldots + \frac{\beta^\infty(B-A)}{2} = \sum_{n=0}^{\infty} \frac{\beta^n(B-A)}{2} \tag{8}$$

This probability distribution is not intended to be used with β values larger or equal than one, because such high values implicitly means that the uncertainty of bound position is larger than the zero-order uncertainty itself.

This new uncertainty distribution is a hybrid approach combining traditional probabilistic representation of uncertainties with other approaches such as interval analysis [30] and probability bounds analysis [16, 42]. It overcomes the limitations of traditional probabilistic representations that may be too deterministic and other representations that may be over-conservative for the purpose of structural identification.

4. Bridge & test description

The bridge used to demonstrate the applicability of the approach proposed is the Langensand Bridge located in Switzerland. This structure has a single span of 80m and is supported by four skewed bearing devices. The girder profile is presented in Figure 4 along with a schematic representation of its boundary conditions. Note that the bridge profile is slightly arched. Therefore, when the girder is bent vertically, it produces a longitudinal displacement at the free end of the bridge. The structure was monitored during construction. Figure 5 presents phase one that was monitored and that is studied in this paper.

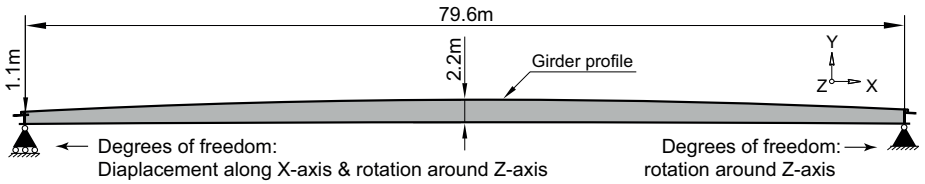

Figure 4: Langensand Bridge elevation representation.

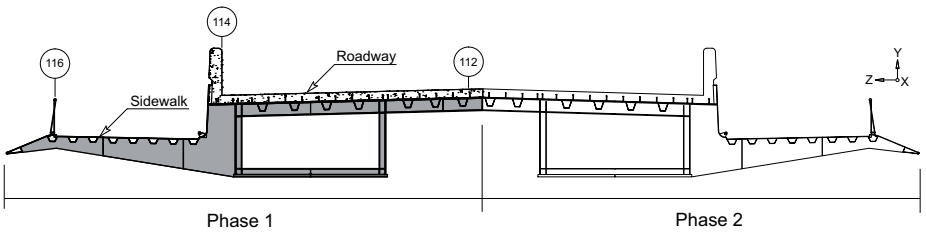

Figure 5: Langensand Bridge cross section. Reprinted from [17] with permission from ASCE

Figure 6 presents the cross-section of the finite element model. This template model

includes the main girder, longitudinal and transverse stiffeners, concrete deck, barriers and rebars and the pavement. These secondary structural elements were included in order to reduce the model simplification errors.

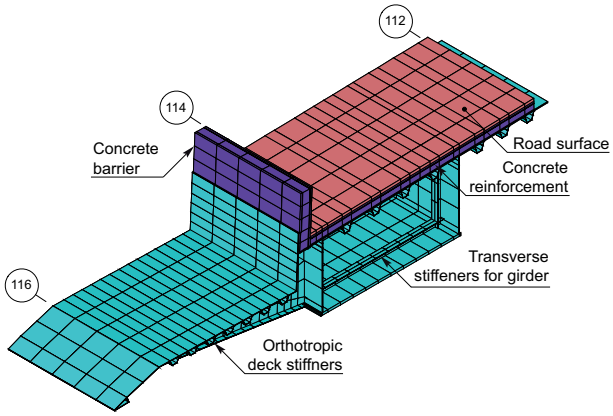

Figure 6: Langensand Bridge template finite element model (Phase 1). Reprinted from [17] with permission from ASCE

A full-scale ambient vibration test has been performed on the bridge by the RCI Dynamics company [10]. 15 channels of PCB 393B31-type accelerometers and a 24-bit central acquisition system (LMS Pimento) were used to record a total of 12 datasets of $30\,\mathrm{min}$ at $100\,\mathrm{Hz}$ sampling frequency. These sensors have a sensitivity of $10^{-6}\,\mathrm{m/s^2}$ between 0.2 and $200\,\mathrm{Hz}$. Two reference 3-component sensors were placed on the bridge deck and the walkway at 47 and $62\,\mathrm{m}$ from the bridge end, respectively. Twelve datasets include a total of 52 recording points using 1 to 3 components (Fig. 7).

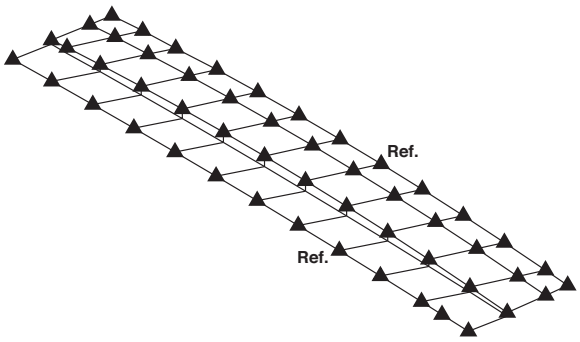

Figure 7: Sensor layout. Each triangle represents a recording point.

5. Ambient vibration recordings processing using Frequency Domain Decomposition

5.1. FDD method

In order to extract the modal parameters of the structure from the ambient vibration recordings, the Frequency Domain Decomposition (FDD) method [8] was chosen. This method was selected because, it decomposes modes while remaining simple enough considering the numerous uncertainties related to modal identification of civil engineering structures [24]. Assumptions underlying this method, are: a white noise input, a low damping ratio and orthogonal close modes. The method has been shown to be robust to the first assumption [28, 29] and the second assumption is generally fulfilled in civil engineering structures. The third assumption, however, is important when dealing with torsion modes. The first step of this method is to calculate the Power Spectral Density (PSD) matrices for each dataset. Given that 15 channels are recorded simultaneously, the size of these matrices is 15x15 for each frequency. The Welch [47] method was used for this purpose, i.e. the modified smoothed periodogram, for which Fourier Transforms of the correlation matrices on overlapping Hamming windows are averaged over the recordings. A STA/LTA algorithm was used to discard signal windows with high energy transients. Only a limited number of modes (frequencies λ_k, mode shape vectors $\{\Phi_k\}$) have energy at one particular angular frequency ω noted $Sub(\omega)$. It can be shown [8] that the PSD matrices of the recordings $[Y](\omega)$ using the pole/residue decomposition take the following form:

$$[Y](j\omega) = \sum_{k \in Sub(\omega)} \frac{\{\Phi_k\} d_k \{\Phi_k\}^T}{j\omega - \lambda_k} + \frac{\{\bar{\Phi}_k\} \bar{d}_k \{\bar{\Phi}_k\}^T}{j\omega - \bar{\lambda}_k} \tag{9}$$

with d_k as constant and $j^2 = -1$. Moreover, a singular value decomposition of the estimated PSD matrices at each frequency can be performed:

$$[\hat{Y}](j\omega) = [V_i][S_i][V_i]^H \tag{10}$$

Identification of Eq. 9 and 10 shows that the modulus of the first singular value gives a peak for an ω value corresponding to a resonance frequency ω_k linked to the continuous-time eigenvalues $\lambda_k = -\xi_k \omega_k \pm j\omega_k \sqrt{1 - \xi_k^2}$ (Fig. 8) [8]. If $Sub(\omega)$ has only one or two geometrically orthogonal elements, the first or the first two singular vectors are proportional to the modal shapes. Moreover, the FDD method can be enhanced (EFDD method) [7] by selecting the Frequency Response Function (FRF) of

the single-degree-of-freedom (SDOF) system corresponding to the mode of interest. The MAC criterion [2] is used for this purpose (Eq. 6). For a MAC values greater than 80%, it is considered that the point still belongs to the FRF of the mode, even on the second singular value. The FRF of the mode is turned into its Impulse Response Function (IRF) by an inverse Fourier Transform. The logarithmic decrement of the IRF gives the damping ratio and a linear regression of the zero-crossing times gives a refined frequency. A decision as to whether or not a peak is a structural mode can be taken by considering the extent of the FRF, the damping ratio and the shape.

In order to estimate uncertainties on a frequency, FDD is back-computed on each selected time window and the distribution of the frequency value at the peak is estimated for all windows of all datasets. It is then fitted by a Gaussian distribution with its mean and standard deviation. The uncertainty related to the EFDD method is provided by the standard deviation of the distribution of results for the 12 datasets and is therefore less reliable.

5.2. Results of the experimental modal analysis

The average FDD spectra of the Langensand bridge recordings are displayed in Figure 8. Averaging reduces the noise in the spectra but may also add peaks related to disturbances present in a sub-set of the data. The relative amplitude of the peaks is meaningless since it depends on the noise input and on the positioning of the sensors. The number of singular values showing a peak at a particular frequency indicates the number of modes having energy at this frequency. For instance, between 7 and 8 Hz, the 3 first singular values show a peak indicating the presence of 3 different modes (Fig. 8).

The modes identified are detailed in Table 1 and the corresponding modal shapes are displayed on Fig. 9. The four first modes of the girder, from 1.26 up to 4.4 Hz, could be easily identified (Fig. 8): first vertical bending, first lateral bending, second vertical bending and first torsion modes. Other peaks in the spectra were not linked to structural behaviour like at 1.8 Hz, where a transient disturbance can be noticed. Moreover, two peaks are found in the spectra in all datasets with the same modal shape corresponding to the first transverse mode Y1, whereas the numerical model indicates it probably corresponds to the same mode. Both were used in the identification method.

Between 7 and 8 Hz, as written above, there should be 3 close modes, but only 2 could be found: the third vertical mode of the girder and a second torsion mode of

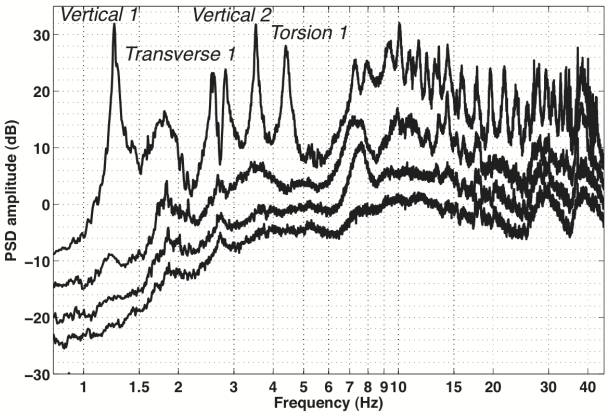

Figure 8: Average FDD spectra of the recordings: 4 first singular values averaged over the 12 datasets.

the girder. Another second torsion mode, affecting mostly the walkway can be found around $9.3\,\mathrm{Hz}$.

Then, from $10\,\mathrm{Hz}$ on, 19 more modes up to $34\,\mathrm{Hz}$ related to the walkway or the bridge bottom flange (not instrumented) were found. They can be correctly interpreted only by comparison with the numerical model.

Table 1: Observed frequencies (f in Hz) and damping ratios (ξ in %) with their standard deviation (σ same unit).

Peak #	Interpretation	FDD method		EFDD method			
		f	σ	f	σ	ξ	σ
1	Vertical 1	1.27	0.02	1.27	0.02	1.2	0.4
2	Transverse 1 peak 1	2.58	0.03	2.59	0.01	1.4	0.2
3	Transverse 1 peak 2	2.83	0.03	2.82	0.01	1.1	0.2
4	Vertical 2	3.53	0.02	3.52	0.01	0.6	0.1
5	Torsion 1	4.40	0.04	4.39	0.01	1.4	0.4
6	Vertical 3	7.29	0.11	7.30	0.04	2.6	0.6
7	Torsion 2a	7.95	0.15	7.99	0.04	3.5	0.6
8	Torsion 2b	9.33	0.15	9.35	0.05	2.1	0.4
9	Walkway 1	10.03	0.12	10.07	0.05	1.5	0.4
10	Walkway 2	10.88	0.15	10.84	0.05	1.0	0.2
11	Walkway 3	11.57	0.11	11.58	0.07	1.0	0.2
12	Walkway 4	12.30	0.11	12.30	0.03	0.7	0.1
13	Walkway 5	13.06	0.10	13.06	0.05	1.1	0.2
14	Walkway 6	13.43	0.05	13.43	0.01	0.3	0.1
15	Walkway 7	14.34	N/A	14.35	N/A	0.52	N/A
16	Walkway 8	14.33	0.07	14.36	0.06	0.9	0.2
17	Walkway 9	15.88	0.08	15.92	0.07	1.6	0.4
18	Walkway 10	17.76	0.09		N/A		
19	Walkway 11	19.60	0.07	19.57	0.07	1.0	0.2
20	Walkway 12	21.72	0.10	21.75	0.07	1.3	0.4
21	Walkway 13	23.64	0.15	23.74	0.12	1.8	0.4
22	Walkway 14	27.72	0.20	27.76	0.21	1.4	0.4
23	Walkway 15	29.48	0.15	29.57	0.16	1.3	0.3
24	Walkway 16	31.12	0.16	31.15	0.09	0.8	0.3
25	Walkway 17	32.77	0.08	32.79	0.06	0.6	0.1
26	Walkway 18	34.05	0.09	34.10	0.04	0.6	0.1
27	Walkway 19	34.83	0.05	34.83	0.03	0.2	0.0

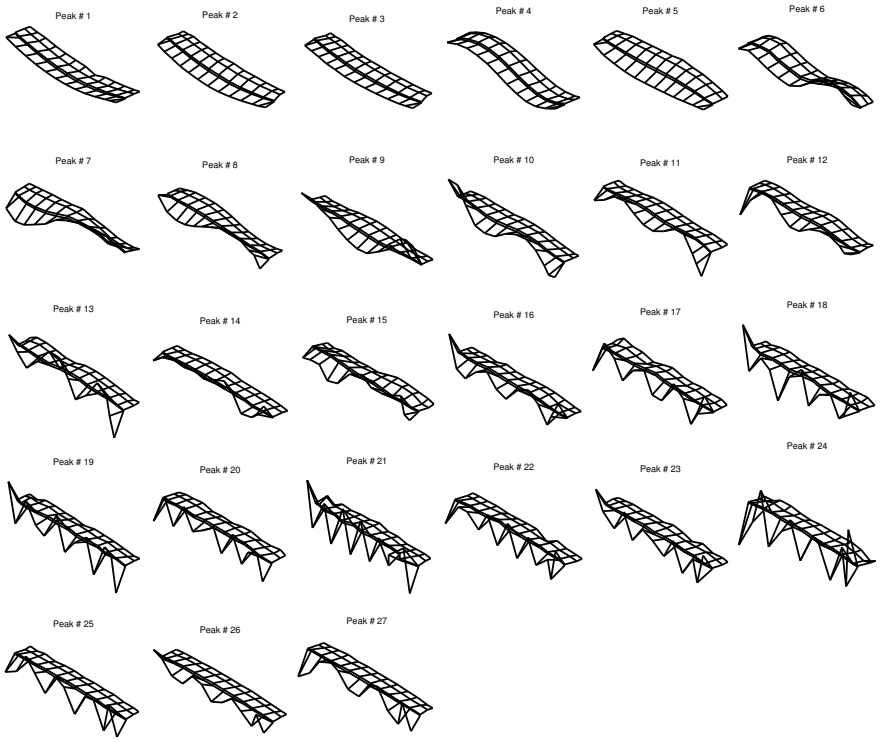

Figure 9: Shapes of the estimated modes

5.3. Variations in the fundamental mode

The results regarding the first recorded mode were unexpected. Even if this mode is theoretically the easiest to measure, it was the least stable along the datasets and it was first found to be at a higher frequency than expected in the model. Therefore, an additional single station measurement was performed nine months later by the company Ziegler Consultants [50] with a 1s velocity sensor. At this time, the traffic was then enabled on the recorded part of the bridge and the second part was already built but not linked to the first one. The comparison of the spectra of the acceleration recordings in the central point of the bridge, between the walkway and the road is displayed on Fig. 10 for the three components. The major differences between these two recordings are in the vertical direction. The level of vertical noise at low frequency ($f < 1\,\mathrm{Hz}$), i.e. representing the static behaviour of the bridge, was much lower during the first measurement (approximately 10 dB) due to the absence of traffic. Moreover, the fundamental frequency drops from 1.27 to $1.17\,\mathrm{Hz}$ (i.e. 8% change, corresponding to a 17% change in stiffness) and the damping ratio increases from 1% to 2%. These differences are explained in the following section using the model identification.

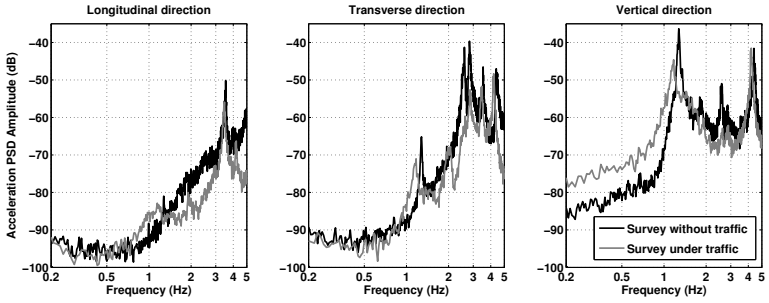

Figure 10: Comparison of two recordings with and without traffic in the centre of the bridge along the 3 axes.

6. Structural identification

Structural identification was performed on the Langensand Bridge using as input the ambient vibration measurements detailed in the previous section. For a predicted mode to be associated with an observed one, the MAC value computed from these two must be larger or equal to $\phi_{\mathrm{MAC}} = 0.8$. Fifteen modes found correspondence between predicted and observed mode shapes. These modes are presented in Figure 11. Model instances for which predicted mode shapes do not pass the MAC correspondence check

for any modes are discarded. Others are classified as either candidate or falsified models, based on the observed residual between the predicted and observed values.

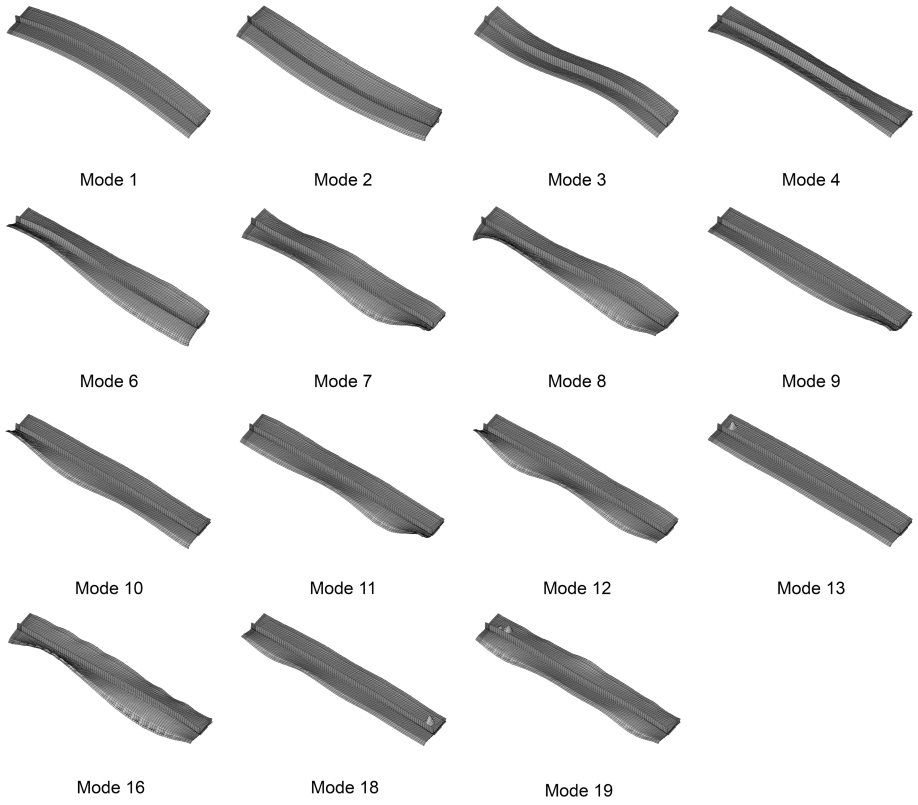

Figure 11: Modes shapes used for the identification

6.1. Initial model set

The initial model set is the discrete representation of the solution space. Primary parameters are those that have ranges of possible values. These ranges have an important effect on predicted frequencies. The template model used to generate model instances (parameter combinations) includes four primary parameters to be identified: the first two are the concrete Young's modulus [20, 45] GPa and the pavement Young's modulus [2, 20] GPa ([ ] is range of possible values). The Young's modulus range includes possible values over the whole structure. For concrete, the range is based on upper and lower bounds for a concrete having a nominal strength of 35 MPa. The range for the pavement stiffness is based on possible values reported for similar materials [35]. The third parameter is the stiffness of the restriction on horizontal expansion

of the structure caused by the formwork [0, 1000]kN/m. This formwork was found during a visual inspection of the structure and an upper bound for it stiffness was estimated in [17]. The fourth parameter is the stiffness of the longitudinal spring added to simulate a movement restriction imposed on the slider bearing devices [0, 2000]kN/m. This range goes from a completely free beading device movement up to a quasi-full restriction. In this case, restraining the longitudinal expansion of the structure influences vertical stiffness especially because its longitudinal profile is slightly arched. The initial model set contains 2400 model instances (combinations of the four parameters to identify). Model instances are generated according to a hyper-grid bounded by the interval of each parameter. All other model parameters have a marginal effect on model response. Therefore, these are classified as *secondary parameters* and the uncertainty on each parameter value is propagated through the model to obtain this contribution to model prediction uncertainty.

6.2. Uncertainties

The expected residual PDF is computed by combining several sources of uncertainty. Uncertainties associated with secondary parameters are presented in Table 2 where the mean and standard deviation are reported for each source. Δ indicates the deviation with respect to the nominal parameter value, v stands for a Poisson ratio, t a thickness and d a density. As mentioned above, secondary parameters are model parameters that have a lesser influence than the primary parameters (parameters to identify).

Table 2: Secondary-parameter uncertainties

Uncertainty source	Unit	Mean	σ
Δv concrete	-	0	0.025
Δt steel plates	%	0	1
Δt pavement	%	0	5
Δt concrete	%	0	2.5
Δ d steel	kg/m^3	7850	25
Δ d concrete	kg/m^3	2400	50
Δ d pavement	kg/m^3	2300	50

Other uncertainty sources are reported in Table 3 where the lower and upper bounds for each uncertainty source is provided. These uncertainty distributions are modeled as an extended uniform distribution (EUD) having a β value of 0.3.

The estimation of the uncertainties in the experimental parameters is not straightforward. A part of the uncertainty is related to the variability of the frequencies themselves and another part is related to errors in the estimations. The long-term natural variations in the frequencies is mostly depending on temperature effects that were negligible during the duration of the tests. Otherwise, temperature effects could cause a 10% variation (or more) in measured values, depending on the structure and test conditions [12, 48]. Variability on shorter time periods are assessed by estimating the distribution of the results along the dataset (see, Table 1) inferred by a Gaussian relationship. The standard deviation does not exceed 2% here. Errors in measurements include the digitization errors (time stamping) that are negligible, the assumption of white noise input and the precision of the modal analysis method used. The assumption of white noise input is robust as shown by Michel et al. [28], with variations lower than 1% even for a short energetic signal. Errors due to the technique used include the precision of the spectral estimation and the mode selection errors that are already included in the variability found across the datasets. Moreover, the error due to the signal processing method itself, FDD here, is in the order of 1% according to Peeters and Ventura [34]. Therefore, an extended uniform distribution ($\beta = 0.3$) with bounds at $\pm 2\%$ of the frequency values are added to the observed variability across the datasets. As a comparison, Lamarche et al. [24] found that the overall uncertainty related to the ambient vibration technique is in the order of 3%, compared with forced vibrations.

Model simplification uncertainty evaluation is based on previous studies [17, 19] that estimated the prediction uncertainty related to degrees of freedom (DOF's) (displacements and rotations) to be between 0% and 7% of the averaged predicted value. Since the natural frequency is proportional to the square of the stiffness, the uncertainty in frequency prediction is estimated to be the square root of the DOF's uncertainty rounded toward the highest integer. Model simplification uncertainty is negative because simplifications and omissions decrease the model stiffness compared with the real structure. Thus, this underestimation of stiffness also leads to lower natural frequencies. Mesh refinement errors are evaluated by refining the mesh of the model until it converges to a stable value. Additional uncertainties are provided to include other minor factors.

Combining all previous sources of uncertainty for each mode leads to the expected residual PDF. The relative importance of uncertainty sources is showed in Figure 12.

Table 3: Other uncertainty sources

Uncertainty source	Frequency min	Frequency max
Measurement variability	See Table 1	
Modal analysis errors	-2%	2%
Model simplifications & FEM	-3%	0%
Mesh refinement	0%	-1%
Additional uncertainties	-1%	1%

The main components of uncertainty are the measurement variability, the uncertainty introduced by secondary parameter uncertainty (Table 2) and model simplifications. Coverage intervals are computed for each mode in order to separate candidate and falsified models with a target reliability, ϕ, equal to 95%.

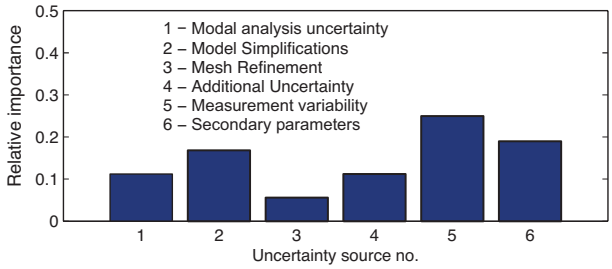

Figure 12: Uncertainty distribution

6.3. Uncertainty dependencies

As mentioned in the introduction, uncertainty dependencies are in many cases, extremely hard to quantify. From all the uncertainty sources presented in the previous section, only the dependence due to the secondary parameter uncertainty can be evaluated when uncertainties are propagated through the template model. The result of this evaluation is presented in Figure 13. The horizontal axes represent the secondary parameter uncertainty for different modes and the height of each bar is the absolute value of the correlation between the two corresponding quantities.

The results presented in this figure show that a high correlation between uncertainties is expected. This does not correspond to the idealized case assumed by traditional approaches where uncertainties are all independent. There are many other uncertainty sources involved in the identification for which the exact dependencies cannot be evaluated. Therefore, using the error-domain model falsification approach is justified since

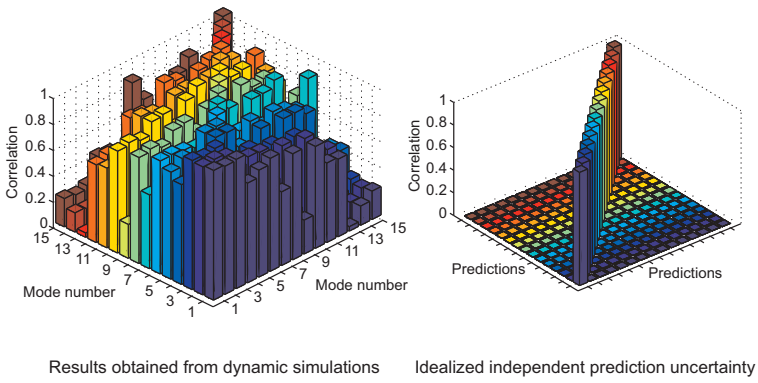

Figure 13: Secondary parameter uncertainty correlation between different vibrating modes

it does not require knowing the dependencies between prediction uncertainties. It provides conservative results no matter what the actual dependencies are.

6.4. Results

Figure 14 compares the scatter in model predictions with the observed frequencies for the first and second modes. Model instances are represented on the horizontal axis and the vertical axis corresponds to either the predicted or measured value. Points represent the falsified models and crosses represent the candidate models. Here, candidate and falsified models are overlapping because models can be accepted by one mode yet rejected by another. The threshold bounds that includes the candidate models is also presented in this figure. The candidate model found all have a partial restriction in the free-movement of bearing devices.

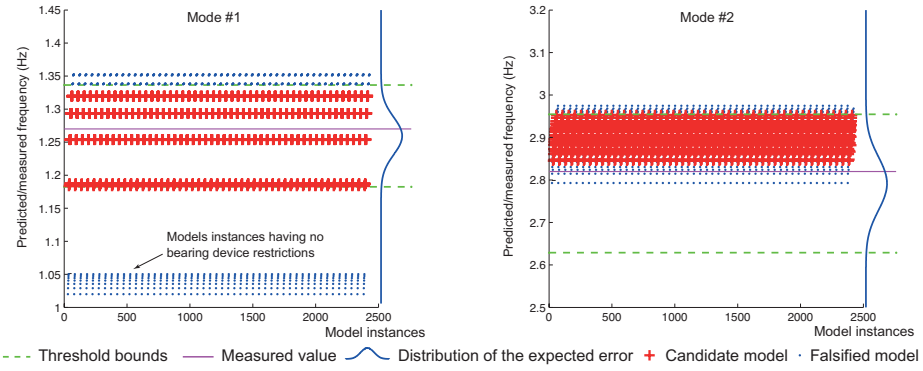

Figure 14: Comparison of the model prediction scatter and measured value for the first two frequencies

The stratified pattern in model prediction for the first frequency is due to the discrete grid sampling used to generate the initial model set. The first frequency is found to be mainly influenced by the bearing device condition. For mode 1, lower frequencies ($1.00 - 1.05\,\mathrm{Hz}$) correspond to either low restriction or free bearing device movement and high frequencies ($> 1.15\,\mathrm{Hz}$) to heavily restricted longitudinal displacement. The candidate models are those within the threshold bounds for all modes. The thresholds falsified all model instance having no restriction ($k = 0\,\mathrm{kN/m}$) for the bearing device movement. Some models with high values of restriction ($k = 2000\,\mathrm{kN/m}$) are also discarded. The effect of the three other parameters is not significant enough compared with the uncertainties to falsify further instances. Therefore, the range of possible parameter values is reduced for the longitudinal bearing device restriction. The number of possible permutations of parameters is reduced from 2400 initial models to 1323 candidate models.

The bearing device hindrance significantly influences only the first frequency of the structure. All higher modes are influenced predominantly by the combined effect of the three other parameters. The scatter in the data is similar to that of the second frequency presented in Figure 14. For the third frequency and higher modes, all models lie within the threshold bounds. Therefore, these modes do not allow the rejection of any model instances.

This shows that results from ambient vibration monitoring may not always be directly interpreted. In this case, small input amplitudes appear to be insufficient to overcome the cohesion and friction allowing the longitudinal movement of the bearing devices. Due to the arched profile of the structure, blocking the longitudinal bearings increases the stiffness significantly in the vertical direction, thereby reducing the fundamental vertical resonance frequency. These conditions inadvertently increased the first natural frequency of the structure by 8% and thereby its apparent stiffness by 17%. Such apparent stiffness was not observed during static measurements because the horizontal forces (caused by truck loading) are high enough to move the bearing devices. Therefore, the refined candidate model set can be used to predict the dynamic behaviour for high and low amplitudes along with its static behaviour.

6.5. Discussion

Results indicate that under ambient vibrations, the bearings are partially blocked. During the second measurement [50], the higher noise level due to the traffic partially

frees the bearings and modifies noticeably the fundamental mode with a decrease in the resonance frequency and an increase in the damping ratio (Fig. 10).

Interpreting the data using an approach that adjusts the structural parameters of the structure in order to minimize the discrepancy between predicted and measured values is dangerous. If wrong assumptions are made at the beginning - for instance if the hypothesis that bearing devices do not work properly under the measured conditions is not included - wrong conclusions could be obtained. In the case of the approach presented here, when the comparison of model instances and measurements was first performed without the hypotheses of bearing device malfunction, all model instances were initially falsified. Such a situation indicated that the model class (template model) used was an inadequate explanation of the observations. The capacity to falsify an entire model class is a unique advantage of this approach.

Conclusions

Error-domain structural identification can be performed using ambient vibration monitoring results as input. The model filtering process is carried out in two steps: firstly a comparison of mode shapes based on MAC value is done to ensure that the same modes are compared; secondly, the frequencies from each model instance are compared with the measurements. The instances for which the difference between the predicted and measured value lie outside the threshold bounds are discarded.

This system identification method is able to show failures in the compatibility between predicted and recorded data. In the case-study presented here, the approach falsified the hypothesis that bearing devices allowed free longitudinal expansion of the structure. Under ambient vibration, the small amplitudes of deformations may not allow the bearing devices to move freely.

Including uncertainties in system identification process is important to avoid misinterpretation of the data. The hybrid probability scheme presented in this paper goes beyond traditional approaches by including uncertainties associated with uncertainty definition. It offers a compromise between conventional statistical descriptions and interval based approaches. This approach to structural identification is proposed as an alternative to more traditional methods, especially for methods that assume that the model class contains the right model.

Acknowledgements

Parts of this paper are an extension of a conference paper presented International Conference on Vulnerability and Risk Analysis and Management/Fifth International Symposium on Uncertainty Modeling and Analysis [18]. This research is funded by the Swiss National Science Foundation under contract no. 200020-117670/1. The authors thank Dr. Cantieni [10] and Dr. Ziegler [50], for the ambient vibration recordings used in this paper. They were made available through the City of Lucerne (Switzerland) and the consulting firm Guscetti & Tournier SA.

[1] A. Abdel-Ghaffar. Dynamic analyses of suspension bridge structures. 1976.

[2] R. Allemang and D. Brown. A correlation coefficient for modal vector analysis. In *Proceedings of the 1st international modal analysis conference*, volume 1, pages 110–116, 1982.

[3] J. Beck and L. Katafygiotis. Updating models and their uncertainties. i: Bayesian statistical framework. *Journal of Engineering Mechanics*, 124(4):455–461, Apr. 1998.

[4] J. Beck and K. Yuen. Model selection using response measurements: Bayesian probabilistic approach. *Journal of Engineering Mechanics*, 130(2):192–203, Feb. 2004.

[5] K. Beven. A manifesto for the equifinality thesis. *Journal of Hydrology*, 320(1-2):18–36, 2006.

[6] K. Beven. *Environmental modelling: an uncertain future?* Routledge, 2009.

[7] R. Brincker, C. Ventura, and P. Andersen. Damping estimation by frequency domain decomposition. In *19th International Modal Analysis Conference*, pages 698–703, 2001.

[8] R. Brincker, L. Zhang, and P. Andersen. Modal identification of output-only systems using frequency domain decomposition. *Smart Materials and Structures*, 10:441, 2001.

[9] J. Brownjohn and P. Xia. Dynamic assessment of curved cable-stayed bridge by model updating. *Journal of Structural Engineering*, 126(2):252–260, Feb. 2000.

[10] R. Cantieni. Langensandbrucke neubau bruckenhalfte seite pilatus - identifikation der eigenschwingungen dynamische belastungsversuche. Technical Report Bericht Nr.081231, RCI Dynamics, Dubendorf, Switzerland, 2008.

[11] D. Carder. Observed vibrations of bridges. *Bulletin of the Seismological Society of America*, 27(4):267, 1937.

[12] F. Catbas, M. Susoy, and D. Frangopol. Structural health monitoring and reliability estimation: Long span truss bridge application with environmental monitoring data. *Engineering Structures*, 30(9):2347–2359, 2008.

[13] F. N. Catbas, S. K. Ciloglu, O. Hasancebi, K. Grimmelsman, and A. E. Aktan. Limitations in structural identification of large constructed structures. *Journal of Structural Engineering*, 133(8):1051–1066, Aug. 2007.

[14] S. H. Cheung and J. L. Beck. Bayesian model updating using hybrid monte carlo simulation with application to structural dynamic models with many uncertain parameters. *Journal of Engineering Mechanics*, 135(4):243–255, Apr. 2009.

[15] M. Cox and B. Siebert. The use of a monte carlo method for evaluating uncertainty and expanded uncertainty. *Metrologia*, 43:S178, 2006.

[16] S. Ferson, J. Hajagos, D. Berleant, J. Zhang, W. Tucker, L. Ginzburg, and W. Oberkampf. Dependence in dempster-shafer theory and probability bounds analysis. Technical Report SAND2004-3072, Sandia National Laboratories, Albyquerque, NM, 2004.

[17] J.-A. Goulet, P. Kripakaran, and I. F. C. Smith. Multimodel structural performance monitoring. *Journal of Structural Engineering*, 136(10):1309–1318, Oct. 2010.

[18] J.-A. Goulet and I. F. C. Smith. Extended unifiorm distribution accounting for uncertainty of uncertainty. In *International Conference on Vulnerability and Risk Analysis and Management/Fifth International Symposium on Uncertainty Modeling and Analysis*, pages P.78–85, Maryland, USA, April 2011.

[19] J.-A. Goulet and I. F. C. Smith. Overcoming the limitations of traditional model-updating approaches. In *International Conference on Vulnerability and Risk Analysis and Management/Fifth International Symposium on Uncertainty Modeling and Analysis*, pages p.905–913, Maryland, USA, April 2011.

[20] JCGM, editor. *Evaluation of measurement data — Guide to the expression of uncertainty in measurement*. ISO/IEC Guide 98-3:2008. JCGM Working Group of the Expression of Uncertainty in Measurement, 2008.

[21] JCGM, editor. *Guide to the Expression of Uncertainty in Measurement Supplement 1: Numerical Methods for the Propagation of Distributions*. ISO/IEC Guide 98-3:2008/Suppl 1:2008. JCGM Working Group of the Expression of Uncertainty in Measurement, 2008.

[22] R. N. Kacker and J. F. Lawrence. Rectangular distribution whose end points are not exactly known: curvilinear trapezoidal distribution. *Metrologia*, 47(3):120–126, June 2010.

[23] H. Khodaparast, J. Mottershead, and M. Friswell. Perturbation methods for the estimation of parameter variability in stochastic model updating. *Mechanical systems and signal processing*, 22(8):1751–1773, 2008.

[24] C. Lamarche, P. Paultre, J. Proulx, and S. Mousseau. Assessment of the frequency domain decomposition technique by forced-vibration tests of a full-scale structure. *Earthquake Engineering and Structural Dynamics*, 37:487–494, 2008.

[25] I. Lira. The generalized maximum entropy trapezoidal probability density function. *Metrologia*, 45(4):L17–L20, Aug. 2008.

[26] C. Mares, J. Mottershead, and M. Friswell. Stochastic model updating: Part 1–theory and simulated example. *Mechanical systems and signal processing*, 20(7):1674–1695, 2006.

[27] V. McLamore, G. Hart, and I. Stubbs. Ambient vibration of two suspension bridges. *Journal of the Structural Division*, 97(10):2567–2582, 1971.

[28] C. Michel, P. Guéguen, and P.-Y. Bard. Dynamic parameters of structures extracted from ambient vibration measurements: An aid for the seismic vulnerability assessment of existing buildings in moderate seismic hazard regions. *Soil Dynamics and Earthquake Engineering*, 28(8):593–604, 2008.

[29] C. Michel, P. Guéguen, S. El Arem, J. Mazars, and P. Kotronis. Full-scale dynamic response of an rc building under weak seismic motions using earthquake recordings, ambient vibrations and modelling. *Earthquake Engineering & Structural Dynamics*, 39(4):419–441, 2010.

[30] R. Moore and F. Bierbaum. *Methods and applications of interval analysis*, volume 2. Society for Industrial Mathematics, 1979.

[31] A. Morassi and S. Tonon. Dynamic testing for structural identification of a bridge. *Journal of Bridge Engineering*, 13(6):573–585, Nov-Dec 2008.

[32] J. Mottershead and M. Friswell. Model updating in structural dynamics: a survey. *Journal of sound and vibration*, 167(2):347–375, 1993.

[33] C. Papadimitriou, J. Beck, and L. Katafygiotis. Updating robust reliability using structural test data. *Probabilistic Engineering Mechanics*, 16(2):103–113, Apr. 2001.

[34] B. Peeters and C. Ventura. Comparative study of modal analysis techniques for bridge dynamic characteristics. *Mechanical Systems and Signal Processing*, 17(5):965–988, 2003.

[35] J. Perret. *Déformations des couches bitumineuses au passage d'une charge de traffic*. PhD thesis, Swiss Federal institute of technology (EPFL), Lausanne, Switzerland, 2003.

[36] K. Popper. *The logic of scientific discovery*. Psychology Press, 2002.

[37] B. Raphael and I. F. C. Smith. Finding the right model for bridge diagnosis. In *Artificial Intelligence in Structural Engineering, Computer Science, LNAI 1454*, pages 308–319. Springer, 1998.

[38] E. Reynders, A. Teughels, and G. De Roeck. Finite element model updating and structural damage identification using omax data. *Mechanical Systems and Signal Processing*, 24(5):1306–1323, 2010.

[39] Y. Robert-Nicoud, B. Raphael, O. Burdet, and I. F. C. Smith. Model identification of bridges using measurement data. *Computer-Aided Civil and Infrastructure Engineering*, 20(2):118–131, Mar. 2005.

[40] M. Sanayei, E. S. Bell, C. N. Javdekar, J. L. Edelmann, and E. Slavsky. Damage localization and finite-element model updating using multiresponse ndt data. *Journal of Bridge Engineering*, 11(6):688–698, Nov-Dec 2006.

[41] H. Schlune, M. Plos, and K. Gylltoft. Improved bridge evaluation through finite element model updating using static and dynamic measurements. *Engineering Structures*, 31(7):1477–1485, July 2009.

[42] K. Sentz and S. Ferson. Probabilistic bounding analysis in the quantification of margins and uncertainties. *Reliability Engineering & System Safety*, 2011.

[43] I. F. C. Smith and S. Saitta. Improving knowledge of structural system behavior through multiple models. *Journal of Structural Engineering*, 134(4):553–561, Apr. 2008.

[44] P. Stark and L. Tenorio. A primer of frequentist and bayesian inference in inverse problems. *Large-Scale Inverse Problems and Quantification of Uncertainty*, pages 9–32, 2010.

[45] A. Tarantola. Popper, bayes and the inverse problem. *Nature Physics*, 2(8):492–494, Aug. 2006.

[46] W. Wang, J. Mottershead, and C. Mares. Mode-shape recognition and finite element model updating using the zernike moment descriptor. *Mechanical Systems and Signal Processing*, 23(7):2088–2112, 2009.

[47] P. Welch. The use of fast fourier transform for the estimation of power spectra: a method based on time averaging over short, modified periodograms. *Audio and Electroacoustics, IEEE Transactions on*, 15(2):70–73, 1967.

[48] Y. L. Xu, B. Chen, C. L. Ng, K. Y. Wong, and W. Y. Chan. Monitoring temperature effect on a long suspension bridge. *Structural Control & Health Monitoring*, 17(6):632–653, Oct. 2010.

[49] K.-V. Yuen, J. L. Beck, and L. S. Katafygiotis. Unified probabilistic approach for model updating and damage detection. *Journal of Applied Mechanics-Transactions of the ASME*, 73(4):555–564, July 2006.

[50] A. Ziegler. Schwingungsmessungen auf der langensandbrücke in luzern. Technical Report no. 1621, Ziegler Consultants, Zurich, Switzerland, 2009.